Flavodoxin-Mediated Electron Transfer from Photosystem I to Ferredoxin-NADP$^+$ Reductase in *Anabaena*: Role of Flavodoxin Hydrophobic Residues in Protein−Protein Interactions†

Guillermina Goñi,‡,§ Ana Serrano,‡,§ Susana Frago,‡ Manuel Hervás,|| José Ramón Peregrina,‡ Miguel A. De la Rosa,|| Carlos Gómez-Moreno,‡ José A. Navarro,|| and Milagros Medina*,‡

Departamento de Bioquímica y Biología Molecular y Celular, Facultad de Ciencias and Institute of Biocomputation and Physics of Complex Systems (BIFI), Universidad de Zaragoza, Zaragoza, and Instituto de Bioquímica Vegetal y Fotosíntesis, Universidad de Sevilla-CSIC, Sevilla, Spain

Received August 27, 2007; Revised Manuscript Received November 13, 2007

ABSTRACT: Three surface hydrophobic residues located at the *Anabaena* flavodoxin (Fld) putative complex interface with its redox partners were replaced by site-directed mutagenesis. The effects of these replacements on Fld interaction with both its physiological electron donor, photosystem I (PSI), and its electron acceptor, ferredoxin-NADP$^+$ reductase (FNR), were analyzed. Trp57, Ile59, and Ile92 contributed to the optimal orientation and tightening of the FNR:Fld and PSI:Fld complexes. However, these side chains did not appear to be involved in crucial specific interactions, but rather contributed to the obtainment of the optimal orientation and distance of the redox centers required for efficient electron transfer. This supports the idea that the interaction of Fld with its partners is less specific than that of ferredoxin and that more than one orientation is efficient for electron transfer in these transient complexes. Additionally, for some of the analyzed processes, WT Fld seems not to be the most optimized molecular species. Therefore, subtle changes at the isoalloxazine environment not only influence the Fld binding abilities, but also modulate the electron exchange processes by producing different orientations and distances between the redox centers. Finally, the weaker apoflavodoxin interaction with FNR suggests that the solvent-accessible region of FMN plays a role either in complex formation with FNR or in providing the adequate conformation of the FNR binding region in Fld.

In the photosynthetic electron transfer (ET)[1] chain of some algae and cyanobacteria grown under low-iron conditions, flavodoxin (Fld) replaces ferredoxin (Fd) in the ET from photosystem I (PSI) to ferredoxin-NADP$^+$ reductase (FNR) (*1*). Recognition and binding between the electron carrier protein Fd or Fld and both PSI (subunits PsaC, PsaD, and PsaE) and FNR are required to achieve efficient ET (*2*−*6*). Electrostatic and hydrophobic interactions have been reported to play an important role in the formation of optimal complexes for efficient ET in these systems (*3*, *7*−*15*). Thus, it is claimed that while electrostatic interactions usually help in the initial recognition processes, hydrophobic interactions bring the two interacting surfaces close enough so that the physiologically competent ET between redox centers can take place. Structures for photosynthetic FNR_{ox}:Fd_{ox} complexes (*16*, *17*), including that of *Anabaena*, confirmed the importance of such interactions. However, the structure for the FNR:Fld complex remains elusive.

Superposition of FNR and Fld coordinates onto the NADPH-cytochrome P450 reductase structure provided a good model for the *Anabaena* FNR−Fld interaction (Figure 1A) (*18*). This model shows Fld binding around the FAD cofactor on the concave side of FNR (Figure 1A), with the molecular dipoles of FNR and Fld nearly collinear and orientated in the same direction. This disposition is identical to that in the crystal structure of the FNR:Fd complex and allows proximity of the redox centers in a nonpolar environment (*16*, *18*). This latter observation suggests that Fld could orientate in different ways on the FNR surface without significantly altering the distance between the methyl groups of FAD and FMN (*4*, *18*). A careful observation of the complex interface suggests that hydrophobic patches located on the FNR and Fld surfaces in the close environment of

† This work has been supported by the Spanish Ministry of Education and Science (Grants BQU2004-00279 to M.M., BIO2003-00627 to C.G.-M., and BMC2003-00458 and BFU2006-01361 to M.A.R.), the Aragonian Government (Grant PIP122/2005 to M.M.), and the Andalusian Government (PAIDI, Grant CVI-0198 to M.A.R.). G.G. was a recipient of a BSCH Fellowship.

* To whom correspondence should be addressed. Phone: 34 976762476. Fax: 34 976762123. E-mail: mmedina@unizar.es.

‡ Universidad de Zaragoza.

§ These authors contributed equally to this work, and both have to be considered as first author.

|| Universidad de Sevilla-CSIC.

[1] Abbreviations: ET, electron transfer; Fd, ferredoxin; Fld, Fld_{ox}, Fld_{sq}, Fld_{hq}, flavodoxin and flavodoxin in its oxidized, semiquinone, and hydroquinone states, respectively; FNR, FNR_{ox}, FNR_{sq}, FNR_{hq}, ferredoxin-NADP$^+$ reductase and ferredoxin-NADP$^+$ reductase in its oxidized, semiquinone, and hydroquinone states, respectively; ApoFld, apoflavodoxin; K_d, dissociation constant; K_a, association constant; k_{ap}, apparent rate constant; k_{et}, first-order electron transfer rate constant; k_{obs}, pseudo-first-order observed rate constant; k_2, second-order rate constant; PSI, PSI_{ox}, PSI_{rd}, photosystem I and photosystem I in its oxidized and reduced states, respectively; WT, wild type; Cytc, horse heart cytochrome *c*.

10.1021/bi7017392 CCC: $40.75
Published on Web 01/05/2008

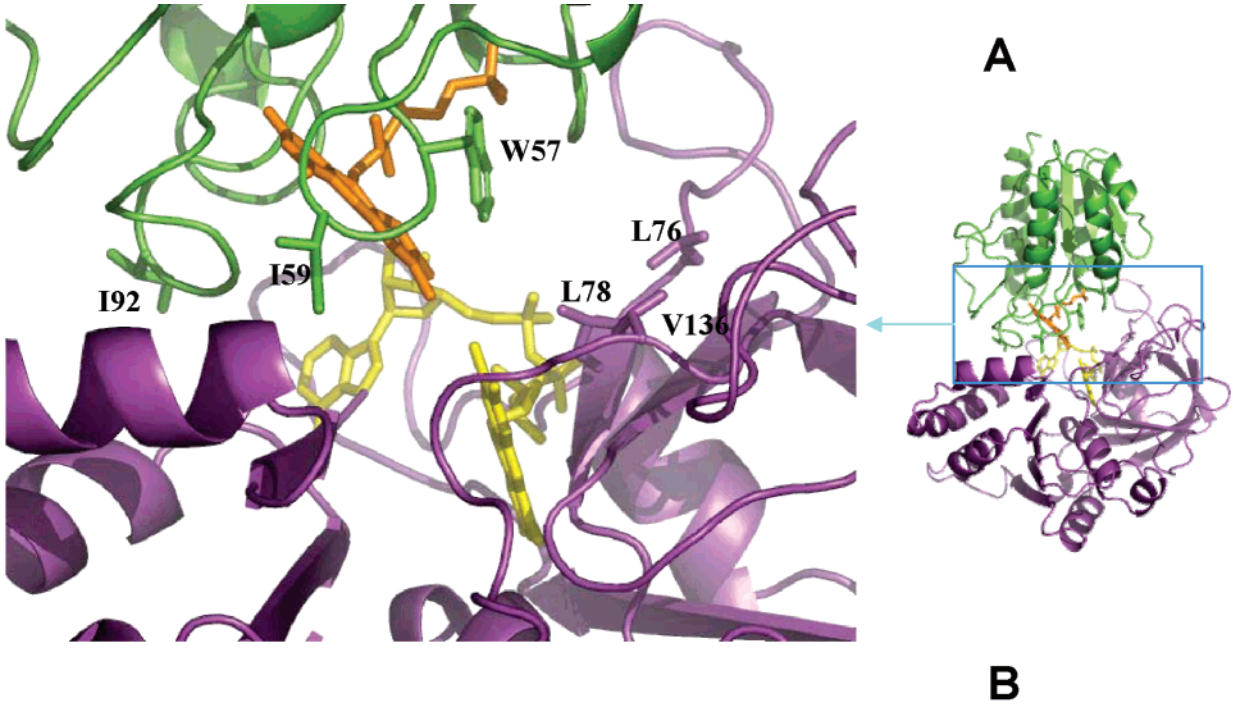


```
.....50.....60.....70.....80.....90.....100
Anabaena sp.          QYLIIGCPTWNIG--ELQ------SDWEGLYS-ELDDVDFNGKLVAYFGTGDQIGYADNFQD
E.coli                DILLLGIPTWYYG--EAQ------CDWDDFFP-TLEEIDFNGKLVALFGCGDQEDYAEYFCD
Sh.flexneri           DILLLGIPTWYYG--EAQ------CDWDDFFP-TLEEIDFNGKLVALFGCGDQEDYAEYFCD
Kl.pneumoniae         DILLLGIPTWYYG--EAQ------CDWDDFFP-TLEEIDFNGKLVALFGCGDQEDYAEYFCD
H.influenzae          DFLLFGIPTWYYG--EAQ------ADWDDFFP-TLEEIDFTDKLVGIFGCGDQEDYADYFCD
B.aphidicola          NFLIFGVPTWYYG--EVQ------CDWDDFLP-TLKKINFSNKIVALFGCGDQEDYSEYFCD
H.pylori              TKVILVAPTAGAG--DLQ------TDWEDFLG-TLEASDFATKTIGLVGLGDQDTYSETFAE
T.erythraeum          QNVIIGCPTWDVG--ELQ------SDWSGFYSEELDNVKFTGKKVAYFGTGDQIGYADNFQD
Synechococcus sp.     DYLIIGCPTWNVG--ELQ------SDWEGIYD-DLDSVNFQGKKVAYFGAGDQVGYSDNFQD
Synechocystis sp.     SCLIIGCPTWNVG--ELQ------SDWEGFYD-QLDEIDFNGKKVAYFGAGDQVGYADNFQD
S.typhimurium         DVLILGIPTWDFG--EIQ------EDWEAVWE-QLDDLNLEGKIVALYGMGDQLGYGEWFLD
A.vinelandii          QFLILGTPTLGEGELPGLSSDCENESWEEFLP-KIEGLDFSGKTVALFGLGDQVGYPENYLD
R.capsulatus          DFLILGTPTLGDGQLPGLSANAASESWEEFLP-RIADQDFSGKTIALFGLGDQVTYPLEFVN
E.agglomerans         PVLLLGTPTLGDGELPGVEAGSQYDSWQEFTN-TLSEADLTGKTVALFGLGDQLNYSKNFVS
Ch.crispus            DLLFLGAPTWNTGADTE-RSG---TSWDEFLYDKLPEVDMKDLPVAIFGLGDAEGYPDNFCD
D.vulgaris            DLVLLGCSTWGDDSIELQ------DDFIPLFD-SLEETGAQGRKVACFGCGDSS-Y-EYFCG
D.gigas               DVVLLGCSTWGDDEIELQ------EDFVPLYE-DLDRAGLKDKKVGVFGCGDSS-Y-TYFCG
D.salexigens          DIVLFGCSTWGEEEIELQ------DDFIPLYD-SLENADLKGKKVSVFGCGDSD-Y-TYFCG
D.desulfuricans       DAVLFGCSAWGMEDLEMQ------DDFLSLFE-EFNRIGLAGRKVAAFASGDQE-Y-EHFCG
C.beijerinckii        DILILGCSAMGDEVLEE-------SEFEPFIE-E-ISTKISGKKVALFGSYGWGD--G---K
C.saccharobuty        EGIIFGTPTYYANISW---------EMKKWID-ESSEFNLEGKLGAAFSTANSIAGGSD--I
A.aeolicus            DGLAVGSPTNMGLVSWKMK-----RFFDDVLG--DLWGEIDGKIACAFSSSGGWGGGNE--V
```

FIGURE 1: (A) Representation of the interaction surface of the *Anabaena* FNR:Fld complex model (*18*). Fld and FNR are represented as cartoons and colored in green and violet, respectively. FMN and FAD cofactors are represented in orange and yellow sticks, respectively. Trp57, Ile59, and Ile92 in Fld and Leu76, Leu78, and Val136 in FNR are represented as sticks. The inset shows a lateral view of the full complex. (B) Sequence alignment of Flds from different sources along the 50's and 90's loops of *Anabaena* PCC 7119 Fld.

their FAD and FMN cofactors contribute to the stabilization of the productive FNR:Fld complex. Additionally, the largest hydrophobic interaction surface in Fld is contributed by the solvent-exposed benzyl portion of FMN. Thus, the side chains of residues Leu76, Leu78, and Val136 in *Anabaena* FNR, key side chains for the formation of optimal complexes with either Fd or Fld (*7*, *10*), are suggested to interact with the Fld Trp57 side chain and the 7- and 8-methyl groups of the benzyl portion of FMN (*18*).

In *Anabaena* Fld, Trp57 plays an important role in setting the structural and electronic environment to allow efficient ET from PSI to FNR (*11*, *19*). This residue, stacking the FMN *re* face, is commonly a Trp, as in *Anabaena* (Figure 1B) (*20*−*24*), but nonaromatic residues are also found in other Fld's (Figure 1B) (*25*−*29*). Two other hydrophobic residues protrude from the Fld surface at the complex interface with FNR, Ile59 and Ile92. Since different FNR:Fld orientations allow close distance between redox cofactors, rotation of the Fld molecule over its dipole moment might produce orientations in which Ile59 or Ile92 would contribute, providing hydrophobic interactions with the hydrophobic patches of FNR (Figure 1A). Residues of very different nature can be found at these positions in Flds (Figure 1B), but in general, they are relatively bulky hydrophobic or negatively charged side chains. The Ile residue found in *Anabaena* Fld is the less common one. Although there are

no high-resolution three-dimensional structures for the PSI-Fd or PSI-Fld interactions, it has been possible to define the PSI docking site for both Fd and Fld at the edge of the three extrinsic PSI subunits PsaC, PsaD, and PsaE (*13*, *15*, *30*, *31*). Mutational analysis indicates that the interaction is driven by positively charged residues on the three subunits as well as by a patch of uncharged residues on the PsaC unit. This patch is solvent-exposed and located close to the terminal Fe/S acceptor cluster (F_B) (*2*, *14*, *15*).

Important modulations of complex formation or ET between Fld and its soluble protein partners were observed upon mutating certain residues (*3*, *7*, *11*, *32*). However, more significant effects were observed in the PSI:Fld system, both in association and in ET (*3*, *7*, *11*). The three *Anabaena* Fld surface hydrophobic residues mentioned above, Trp57, Ile59, and Ile92, are located at the loops involved in FMN isoalloxazine binding and in the putative FNR interaction site (Figure 1A). In the present work we have used several Flds mutated at these positions to provide further insights into their role in Fld interaction and ET with both FNR and PSI. The role of Trp57, at the loop stacking the inner face of the isoalloxazine ring, has been analyzed by using mutants where the Trp57 has been replaced by either positively or negatively charged residues, namely, Trp57Lys, Trp57Arg, and Trp57Glu. Moreover, the role of the two hydrophobic side chains at the 50's and 90's loops, Ile59 and Ile92, which are spread on the Fld surface at the putative interface with FNR (Figure 1A), has been analyzed by either individually or simultaneously replacing their side chains with Ala or Glu (Figure 1). None of the introduced substitutions appears to alter the overall folding of *Anabaena* Fld, but mutations at Trp57, Ile59, and Ile92 modulate the affinity of the diverse redox states of FMN for ApoFld, as well as the $E_{ox/sq}$ and $E_{sq/hq}$ potentials of Fld (*19*, *33*). Finally, because previous analysis of the FNR−Fld interaction model suggested the involvement of the hydrophobic benzyl portion of the Fld flavin cofactor, as well as the possibility of different orientations of the Fld on the FNR surface without significantly altering the distance, orientation, and interaction surface between the methyl groups of FAD and FMN (*4*, *18*), the involvement of FMN in providing a strong FNR−Fld interaction has been tested by using the apoflavodoxin (ApoFld) form from *Anabaena* Fld. The structure of this ApoFld displays a compact fold (*34*). Removal of the cofactor induces changes limited to the cofactor binding region, allowing the indole ring of Trp57 to close the depression previously occupied by the pyrimidine portion of the isoalloxazine ring and by the ribityl moiety of FMN.

MATERIALS AND METHODS

Sequence Alignment. Sequences of long-chain Flds obtained with a BLAST search were aligned using ClustalW over the *Anabaena* PCC 7119 Fld sequence (the final alignment was visually refined).

Biological Material. *Anabaena* PCC 7119 Fld mutants at Trp57, Ile59, and Ile92 were produced by using the QuikChange site-directed mutagenesis kit from Stratagene in combination with synthetic oligonucleotides (*33*). Mutations were verified by DNA sequence analyses and MALDI-TOF. The pTrc99a vectors containing the mutated Fld gene were transformed into *Escherichia coli* TG1. Recombinant WT FNR, WT Fld, and Fld mutants were purified from Luria−Bertani cultures of IPTG-induced *E. coli* cells (*11*). UV−vis spectra and SDS−PAGE were used as purity criteria. ApoFlds were prepared by treating Fld with 3% trichloroacetic acid at 4 °C in the presence of 1 mM dithiothreitol. The precipitated apoprotein was separated from FMN by centrifugation (*35*). Precipitated ApoFld was dissolved in 500 mM Tris/HCl, pH 8.0, and dialyzed against 50 mM Tris/HCl, pH 8.0.

Spectral Analysis. UV−vis spectra were obtained on a Kontron Uvikon 942, an Agilent HP 8453, or a Varian Cary 100 Bio spectrophotometer. Dissociation constants (K_d), extinction coefficient changes ($\Delta\epsilon$), and free energy changes ($\Delta G°$) for the complexes between WT FNR_{ox} and the different Fld_{ox} forms were obtained at 25 °C in 50 mM Tris/HCl, pH 8.0, by difference absorption spectroscopy (*11*, *36*). Fitting of the experimental data to the theoretical equation for a 1:1 complex allowed the calculation of K_d and $\Delta\epsilon$. Values were obtained from 2−4 different experiments. Errors in the estimated K_d and $\Delta\epsilon$ values were ±15%, and that for $\Delta G°$ was ±10%. The FNR-dependent NADPH-cytochrome *c* reductase activity was assayed by using the different Fld forms as electron carrier from FNR to horse heart cytochrome *c* (Cytc) (Sigma) at 25 °C, in 50 mM Tris/HCl, pH 8.0 (*36*). Values were obtained from 2−4 different experiments. Errors in the estimated K_m and k_{cat} values were ±15% and ±10%, respectively. Extinction coefficients used for quantification were 9400 M^{-1} cm^{-1} at 458 nm for FNR_{ox} (*37*) and those previously reported for the different Fld forms (*33*).

Stopped-Flow Kinetic Measurements. Stopped-flow experiments were carried out under anaerobic conditions using an Applied Photophysics SX17.MV spectrophotometer as previously described (*11*, *36*). Reduced samples of FNR and Fld were prepared by photoreduction with 5-deazariboflavin. Reactions between FNR and Fld were followed at 600 nm after the proteins were mixed at a ∼1:1 molar ratio, with a final concentration of ∼10 μM each. Reactions between Fld_{hq} and Cytc were followed at 550 nm, with a final concentration of ∼10 μM for each protein. All reactions were carried out in 50 mM Tris/HCl, pH 8.0. Processes between FNR and Fld were followed at 10 °C and those between Cytc and Fld at 25 °C. The apparent observed rate constant values (k_{ap}) were calculated by fitting the data to mono- or biexponential processes. Values for kinetic constants were obtained from 10−12 different kinetic traces under the same conditions. Estimated errors in the determined values were ±15%.

Laser-Flash Absorption Spectroscopy. ET processes between PSI and Fld were studied by laser-flash absorption spectroscopy by following the absorbance changes at 580 nm as previously described (*11*, *38*). The standard reaction mixture contained, in a final volume of 1 mL, 20 mM Tricine/KOH, pH 7.5, 0.03% β-dodecyl maltoside, an amount of PSI-enriched particles equivalent to 35 μg of chlorophyll mL^{-1}, 0.1 μM phenazine methosulfate, 2 mM $MgCl_2$, 2 mM sodium ascorbate, and Fld at the indicated concentration. The experiments at different $MgCl_2$ concentrations were carried out under the same conditions with a final Fld concentration of 20 μM. Each kinetic trace was the average of 40−50 measurements, with 30 s time spacing between flashes (*39*). Values for kinetic constants were obtained from 2−3 different experiments. Kinetic analyses were carried out according to the two-step reaction mechanism previously

Table 1: Steady-State Kinetic Parameters for the Fld−FNR Interaction: NADPH-Dependent Cytochrome *c* Reductase Activity of WT FNR Using WT and Mutated Fld Forms from *Anabaena* PCC 7119 as the Electron Carrier and Dissociation Constants, Extinction Coefficient Changes at Band I, Position of Flavin Bands in the Difference Spectra, and Free Energy for Complex Formation of WT FNR_{ox} with WT and Mutated Fld_{ox} Forms

Fld form	k_{cat}^{Fld} (s^{-1})	K_m^{Fld} (μM)	k_{cat}/K_m^{Fld} ($\mu M^{-1} s^{-1}$)	K_d (μM)	$\Delta\epsilon_{band\ I}$ ($M^{-1} cm^{-1}$)	band II (nm)	band I (nm)	$\Delta G°$ (kcal mol^{-1})
WT[a]	23.3	33.0	0.70	3.0	1.4	394	462	−7.5
W57E	13.8	70.1	0.20	40.3	1.76	385	460	−6.0
W57K	90.3	89.1	1.01	31.0	2.0	386	459	−6.1
W57R	52.7	76.7	0.69	19.7	1.4	384	457	−6.4
W57F[b]	37.0	39.0	1.0	4.0	1.0			−7.4
W57A[b]	18.0	12.0	1.5	4.5	1.0			−7.4
W57L[b]	20.0	21.0	1.0	2.8	1.2			−7.5
W57Y[b]	36.0	27.0	1.4	2.2	2.0			−7.7
I59A	19.0	8.0	2.38	4.7	3.0	387	465	−7.3
I59E	27.5	8.9	3.09	2.5	2.3	392	466	−7.6
I92A	25.8	8.2	3.15	8.0	2.6	385	463	−6.9
I92E	26.5	9.6	2.77	5.0	3.9	385	463	−7.2
I59A/I92A	15.3	33.8	0.45	7.1	3.6	385	462	−7.0
I59E/I92E	14.0	40.0	0.35	7.2	2.6	385	462	−7.0
ApoFld				72.0	0.3	401	461	−5.6

[a] Data from ref *36*. Control WT data were again determined in the present study, obtaining values similar to those reported. [b] Data from ref *11*.

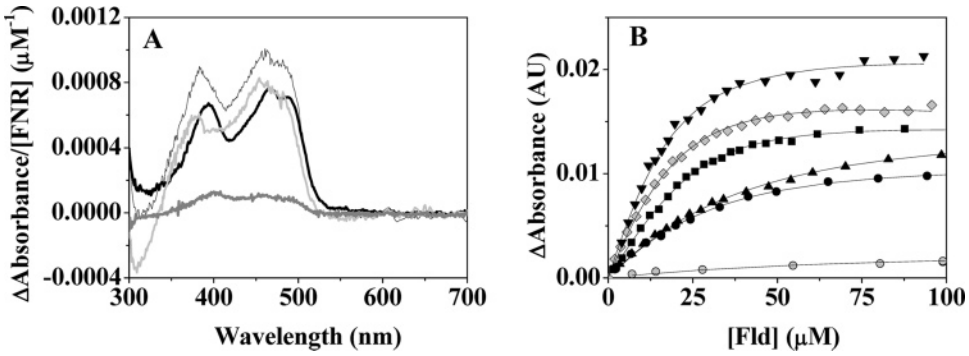

FIGURE 2: Spectroscopic characterization of WT FNR_{ox}:Fld_{ox} complexes: (A) difference absorption spectra elicited by the binding to WT FNR_{ox} of WT (147 μM) (bold line), Trp57Lys (158 μM) (thin line), and Trp57Arg (108 μM) (thin light gray line) Fld_{ox} and ApoFld (237 μM) (bold light gray line), (B) titration of WT FNR with WT (filled squares), Trp57Lys (filled triangles), Trp57Arg (filled circles), Ile92Ala (filled gray tilted squares), and Ile59Ala/Ile92Ala (filled upside-down triangles) Fld and ApoFld (filled gray circles). Fittings for a 1:1 interaction are shown.

proposed (*39*, *40*). For most experiments, the estimated error in the observed rate constants (k_{obs}) was less than 20%, on the basis of reproducibility and signal-to-noise ratios.

Calculation of the Surface Electrostatic Potential and Dipole Moment. On the basis of the *Anabaena* Fld three-dimensional structure (PDB entry 1flv), in silico models for the different Fld mutants were generated using the mutation tool implemented in SPDB-Viewer 3.7 (*41*). Subsequent energy minimization was done using the AMBER suite of molecular dynamics simulations and the AMBER force field (*33*, *42*). The partial charge on each atom of the FMN cofactor was taken from ref *43*. The H++ software (*44*, *45*) was used to protonate hydrolizable residues. The rmsd for all atoms of the molecules modeled with regard to WT Fld was under 0.2 Å when far from the introduced mutations (*33*). Electrostatic surface potentials were calculated for each Fld variant with SPDB-Viewer 3.7 (*41*). The dipole moment (μ) for WT and mutated Flds has been calculated by using the equation $\mu = \sum q_i r_i$, where q_i and r_i stand for the partial charge and the coordinates, respectively, of each protein atom. The center of mass of each protein was used as a reference position for the calculation of μ.

RESULTS

Steady-State Kinetic Analysis of the Different Fld Mutants. The cytochrome *c* reductase activity of FNR was assayed using different Fld mutants as electron carriers from FNR to Cytc (Table 1). Introduction of a positive charge at the position of Trp57 increased both the FNR k_{cat} (2- and 4-fold for Trp57Arg and Trp57Lys, respectively) and K_m^{Fld} (by ∼3-fold) (Table 1). This suggests slightly weaker interactions but faster ET processes between FNR and these Fld mutants. Combination of both effects resulted in similar FNR catalytic efficiencies (k_{cat}/K_m) when using Trp57Arg or WT Fld, while the efficiency was slightly improved when using Trp57Lys Fld. Introduction of a negatively charged side chain at Trp57 decreased the FNR k_{cat} by 2-fold and increased the K_m^{Fld} by the same factor. Thus, the system involving Trp57Glu Fld showed a smaller catalytic efficiency (3.5-fold) than that of WT Fld (Table 1), suggesting a less effective interaction. Single Fld mutants at positions 59 and 92 showed FNR k_{cat} values similar to those of WT Fld but considerably lower than FNR K_m^{Fld} (∼4-fold). This suggests that these mutants are more efficient than WT Fld in accepting electrons from FNR (Table 1). Simultaneous replacement at positions 59 and 92 with either Ala or Glu produced a slight decrease in

FNR k_{cat}, whereas the K_m^{Fld} values were similar to that for WT Fld. Therefore, their catalytic efficiency was about 2 times lower than that for WT Fld (Table 1).

Interaction of Fld_{ox} Variants with FNR_{ox}. The spectral changes observed upon titration of WT FNR_{ox} with WT Fld_{ox}, producing a difference spectrum with absorption maxima around 394 and 465 nm, arise from alteration of the FNR_{ox} flavin environment upon Fld association (*11*, *36*). Similar spectral perturbations were observed when the interaction between WT FNR and most of the Fld_{ox} mutants was analyzed. However, mutations showed shifts in the position of the flavin band maxima (Figure 2A, Table 1). This suggests slightly different orientations of the Fld, by a change of the side chain or by a rotation of the protein, around the FAD environment of FNR upon complex formation as a result of the mutation. The magnitude of the difference spectra upon FNR_{ox} titration with Fld_{ox} mutants reached saturation (Figure 2B), allowing determination of the dissociation constants (K_d) and binding energies ($\Delta G°$) for the complexes (Table 1). Mutants at positions 59 and 92 induced a slight weakening of the $FNR_{ox}-Fld_{ox}$ interaction (K_d values within a factor of 2.5 of that with WT Fld), whereas considerably larger effects were observed with mutants at position 57. The K_d values for the interaction of FNR_{ox} with Trp57Glu, Trp57Lys, and Trp57Arg Flds were increased up to 13.3-, 10-, and 6.6-fold, respectively, relative to that of WT Fld (Table 1). The calculated $\Delta\epsilon$ value for the mutant Trp57Arg was similar to that of WT Fld, but considerably increased (up to almost 3 times in some of the Ile59 and Ile92 mutants) for the rest of the mutants (Table 1). Finally, the role of the large hydrophobic solvent-accessible portion of FMN and the conformation of its environment in Fld in providing stabilizing interactions with the hydrophobic regions of FNR (Figure 1A) was evaluated by titrating WT FNR_{ox} with ApoFld. The observed difference spectra (Figure 2A) indicated ApoFld accommodation in the FNR cavity around the FAD cofactor, but K_d values clearly point out a considerably weaker interaction (Table 1).

Fast Kinetic Analysis of the Reaction between Fld Mutants and FNR or Cytc. Fast ET processes between FNR and Fld were studied using anaerobic stopped-flow methodology by following the formation of both protein semiquinone species at 600 nm (*11*). The physiological reaction between WT FNR_{ox} and WT Fld_{hq} occurs mainly within the dead time of the instrument (*36*), a behavior also observed for reactions involving Fld mutations of Ile59 and Ile92 (Table 2). However, considerably slower reactions were observed when Trp57 was replaced with a charged residue (Table 2, Figure 3A). The kinetic traces fit well to a two-exponential process, an observation consistent with the initial formation of both semiquinone species, followed by reduction of FNR_{sq} by Fld_{hq}, as previously suggested for other Fld mutants (*7*).

The reverse process, the oxidation of WT FNR_{hq} by WT Fld_{ox}, is relatively slow and resolved in two phases, assigned to formation of both semiquinones by ET from FNR_{hq} to Fld_{ox}, followed by reduction of a second Fld_{ox} molecule to the semiquinone state by accepting one electron from the FNR_{sq} formed in the first reaction (*3*, *7*, *11*). A two-exponential process with two phases of similar amplitude was also detected for the Fld mutants herein analyzed (Figure 3B). However, different kinetic behaviors were observed among them. Replacement of Ile59 and Ile92 with any residue and of Trp57 with Glu resulted in k_{ap1} and k_{ap2} values within a factor of 3 of those of the WT. More effective ET processes took place upon replacement of Trp57 with a positively charged residue, resulting in an increase of the k_{ap1} values by 1 order of magnitude (Table 2).

Table 2: Fast Kinetic Parameters for the ET Reactions of WT and Mutated Fld Forms with WT FNR Determined by Stopped-Flow Methodology[a]

	k_{ap} (s^{-1}) for the mixing of FNR_{ox} with Fld_{hq}		k_{ap} (s^{-1}) for the mixing of FNR_{hq} with Fld_{ox}	
Fld form	k_{ap1}	k_{ap2}	k_{ap1}	k_{ap2}
WT[b]	nd[c]		2.5	1.00
W57E	120	16.5	2.9	0.51
W57K	65.4	20.2	21.5	2.11
W57R	86.2	18.5	30.7	2.66
W57F[d]	35.0		12.9	1.9
W57A[d]	>600	146	14.0	0.5
W57L[d]	>600		3.8	2.3
W57Y[d]	34.0		5.1	0.8
I59A	nd[c]		2.8	1.4
I59E	nd[c]		7.7	1.9
I92A	nd[c]		2.9	0.5
I92E	nd[c]		2.0	0.6
I59A/I92A	nd[c]		2.5	1.76
I59E/I92E	nd[c]		6.0	1.5

[a] Reaction followed at 600 nm. [b] Data from ref *36*. WT data were again determined in the present study, obtaining values similar to those reported. [c] Reaction occurred within the instrumental dead time. [d] Data from ref *11*.

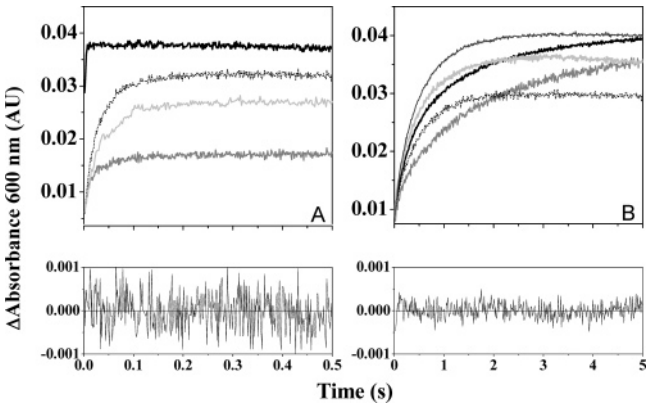

FIGURE 3: Time course for the anaerobic reactions between WT FNR and selected Fld mutants measured by stopped-flow methodology: (A) reaction of WT FNR_{ox} with WT (bold line), Trp57Glu (gray line), Trp57Lys (dotted line), and Trp57Arg (light gray line) Fld_{hq}, (B) reaction of WT FNR_{hq} with WT (bold line), Trp57Glu (gray line), Trp57Lys (dotted line), Ile59Glu (light gray line), and Ile59Glu/Ile92Glu (dark gray line) Fld_{ox}. Residuals for fittings of the Trp57Lys Fld processes are shown at the bottom.

To elucidate whether the changes observed in the FNR k_{cat} values obtained by measuring the NADPH-cytochrome *c* reductase activity when using the Fld mutants could be due to the less efficient ET between Fld and Cytc, fast kinetic reactions between the different Fld_{hq} mutants and $Cytc_{ox}$ were analyzed (*7*). When the different Fld_{hq} mutants reacted with $Cytc_{ox}$, an increase in the absorbance at 550 nm was observed due to $Cytc_{ox}$ reduction. In all cases the process was best fit by two exponentials, consistent with the production of $Cytc_{rd}$ and Fld_{sq} and subsequent reduction of a second $Cytc_{ox}$ molecule by Fld_{sq}, as reported for the WT (*3*, *7*). Moreover, the corresponding k_{ap1} and k_{ap2} determined for the reactions

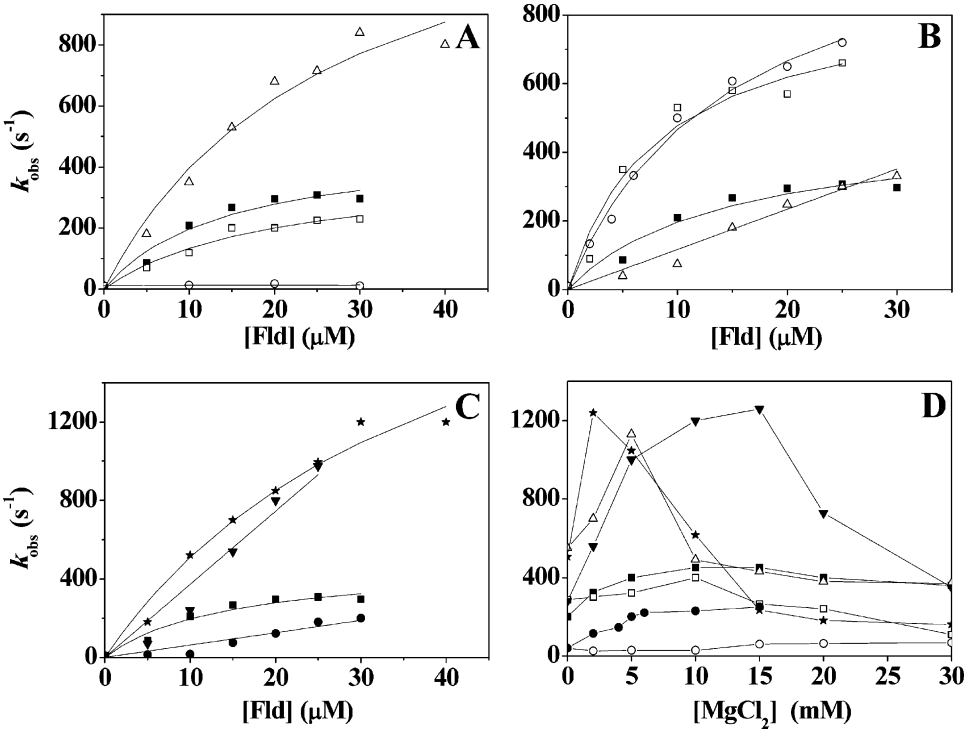

FIGURE 4: Dependence of k_{obs} for Fld_{ox} reduction by PSI_{rd} on the Fld concentration: (A) reduction of WT (filled squares), Trp57Glu (open circles), Trp57Lys (open triangles), and Trp57Arg (open squares) Flds by *Anabaena* PSI, (B) reduction of WT (filled squares), Ile59Ala (open circles), Ile92Ala (open triangles), and Ile59Ala/Ile92Ala (open squares) Flds by *Anabaena* PSI, (C) reduction of WT (filled squares), Ile59Glu (filled upside-down triangles), Ile92Glu (filled circles), and Ile59Glu/Ile92Glu (filled stars) Flds by *Anabaena* PSI, (D) effect of $MgCl_2$ on the k_{obs} for the reduction of WT (filled squares), Trp57Glu (open circles), Trp57Lys (open triangles), Trp57Arg (open squares), Ile59Glu (filled upside-down triangles), Ile92Glu (filled circles), and Ile59Glu/Ile92Glu (filled stars) Flds by PSI_{rd}.

with the different mutants were all within a factor of 2 of those for the processes with WT Fld. Therefore, the mutations introduced in *Anabaena* Fld did not appear to alter the ET between Fld and Cytc.

Kinetic Analysis of the Reduction of Fld Variants by PSI. Although it is widely accepted that the Fld_{sq}/Fld_{hq} couple is the one involved in shuttling electrons between PSI and FNR, a physiological role for the Fld_{ox}/Fld_{sq} couple cannot be precluded (*2*, *15*). Therefore, reduction of *Anabaena* Fld_{ox} to the semiquinone state by PSI_{rd} using laser-flash absorption spectroscopy constitutes a useful model to analyze the interaction forces and ET parameters involved in the physiological reaction (*3*, *11*). Fld mutants showed monoexponential kinetic traces in the reduction by PSI_{rd}, as reported for the WT (*38*), with the exception of Trp57Glu Fld_{ox}, whose reduction was highly impaired. Also similarly to WT Fld, the observed pseudo-first-order rate constants (k_{obs}) for the reduction of Trp57Lys, Trp57Arg, Ile59Ala, Ile59Ala/Ile92Ala, and Ile59Glu/Ile92Glu Flds by PSI_{rd} showed a nonlinear dependence on the Fld_{ox} concentration and a saturation profile. This suggests the formation of a transient PSI_{rd}:Fld_{ox} complex prior to ET (*38*, *46*):

$$PSI_{rd} + Fld_{ox} \overset{K_a}{\rightleftharpoons} PSI_{rd}{:}Fld_{ox} \xrightarrow{k_{et}} PSI_{ox} + Fld_{sq}$$

From the nonlinear dependencies of k_{obs} on the Fld concentration, minimal values for both the association constant for complex formation (K_a) and the ET first-order rate constant (k_{et}) can be inferred (Figure 4 and Table 3) (*40*). Replacement of Trp57 with Lys produced a decrease in the K_a of 1 order of magnitude relative to that of WT Fld, whereas this mutant accepted electrons from PSI_{rd} 4 times faster. On the contrary, introduction of an Arg at the same position only produced a moderate decrease in the interaction with PSI_{rd} and ET parameters (Figure 4A, Table 3).

Table 3: Kinetic Parameters for the Reduction of *Anabaena* WT and Mutated Fld_{ox} Forms by PSI_{rd}[a]

Fld form	K_a (M^{-1})	k_{et} (s^{-1})	k_2[b] ($M^{-1}\,s^{-1}$)
WT[c]	6×10^5	500	
W57E			$<1.0 \times 10^5$
W57K	7×10^4	2060	
W57R	1.3×10^5	362	
W57F[c]	3×10^5	2950	
W57A[c]	6×10^5	1480	
W57L[c]	1×10^5	950	
W57Y[c]	4×10^5	105	
I59A	3.8×10^5	1136	
I59E			3.7×10^7
I92A			1.2×10^7
I92E			6.6×10^6
I59A/I92A	1.6×10^5	853	
I59E/I92E	1.7×10^6	2360	

[a] Reaction followed at 580 nm. [b] k_2 = second-order rate constant. [c] Data from ref *11*. WT data were again determined in the present study, obtaining values similar to those reported.

Replacement of Ile59 and Ile92, either individually or simultaneously, produced noticeable different effects that depend on the mutated position and the introduced residue (Figure 4B,C). Actually, replacement of Ile92 by Ala produced a linear dependence of k_{obs} on the Fld concentration (Figures 4B), suggesting a collisional-type mechanism without formation of a kinetically detectable complex only

characterized by a second-order rate constant, k_2 (*46*):

$$PSI_{rd} + Fld_{ox} \xrightarrow{k_2} PSI_{ox} + Fld_{sq}$$

However, single replacement of Ile59 by Ala only slightly affected the Fld_{ox} affinity for PSI_{rd}, but considerably increased k_{et} (Figure 4B, Table 3). Simultaneous introduction of Ala in these two positions produced a Fld_{ox} that behaved very similarly to the single Ile59Ala Fld (Figure 4B, Table 3). Upon individual replacement of Ile59 or Ile92 by Glu, the k_{obs} values for Fld_{ox} reduction by PSI_{rd} were linearly dependent on the protein concentration (Figure 4C), suggesting again a collisional mechanism. However, whereas the k_{obs} values for Ile92Glu Fld at high Fld concentration indicated a less efficient ET than in the WT (Table 3), considerably larger k_{obs} values were observed for Ile59Glu Fld when the Fld concentration was increased (Figure 4C). Simultaneous introduction of Glu at positions 59 and 92 produced a Fld_{ox} able to bind PSI_{rd} similarly to WT Fld, but increasing the ET rate by a factor of 4.5 (Table 3, Figure 4C). Therefore, the ET rate constant was not drastically different for Ile59Glu and Ile59Glu/Ile92Glu.

Taking into account the electrostatic nature of the *Anabaena* $PSI_{rd}-Fld_{ox}$ interaction (*38*), the effects of charge mutations were analyzed at different $MgCl_2$ concentrations (Figure 4D). The k_{obs} profiles presented a biphasic dependence for all the mutants, as reported for the WT protein (*38*). This bell-shaped salt dependence has been explained as the initially formed electrostatic complex not being optimal for ET. Therefore, the initial interaction would require a rearrangement that could be prevented by the strong electrostatic forces acting at low ionic strength (*39*). Considerable differences were found in both the magnitude and the position of the k_{obs} maxima, regarding the salt concentration (Figure 4D). Trp57Lys, Ile59Glu, and Ile59Glu/Ile92Glu Flds were notably more efficient than WT Fld in most of the $MgCl_2$ range, especially at each maximum. Moreover, in Trp57Lys and Ile59Glu/Ile92Glu the maximum k_{obs} was clearly shifted to a lower $MgCl_2$ concentration. Finally, replacements of Trp57 with Arg, or especially Glu, and Ile92 with Glu produced Fld forms considerably less efficient than the WT in accepting electrons from PSI_{rd} in all the $MgCl_2$ range, and slight displacements of their maxima were also observed (Figure 4D).

DISCUSSION

Long-range electrostatic forces are the major driving force in bringing proteins together before they collide to form protein−protein encounter ET complexes, while specific interprotein salt bridges, hydrophobicity, and desolvation reorient the proteins to form the final productive ET complex (*9*, *46*, *47*). The data reported for the interaction of *Anabaena* Fld with FNR and PSI suggest that its ET efficiency cannot be explained in terms of a single tightly bound productive ET complex addressed by specific electrostatic interactions (*3*). Additionally, it is also of interest to analyze the role of the Fld FMN cofactor and of hydrophobic surface residues, namely, Trp57, Ile59, and Ile92, in guiding the reorientation of encounter complexes to final productive interactions with both of its protein partners, PSI and FNR.

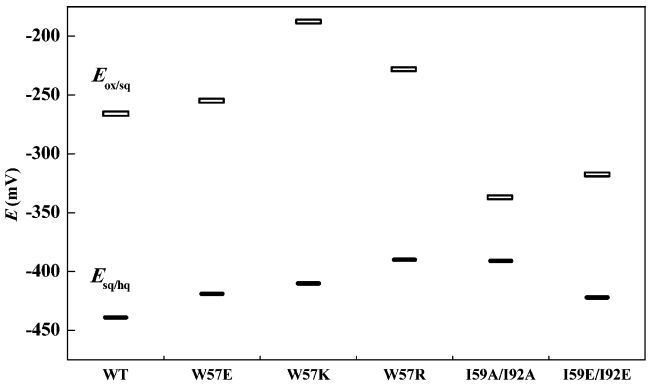

FIGURE 5: $E_{ox/sq}$ and $E_{sq/hq}$ midpoint potentials (mV, pH 8.0) for the WT and the different *Anabaena* Fld mutants (*33*).

Replacement of Trp57 with Lys, Arg, or, especially, Glu produced a weakening of the Fld ability to interact with FNR (Table 1) that was accompanied by a slightly different orientation between the Fld and the FNR flavin rings (Figure 2A). This is consistent with the isoalloxazine surface being more accessible to the solvent when Fld is free (*33*) and, therefore, more accessible to FNR when complexed, allowing new orientations between the flavin rings. Comparison of the surface electrostatic potentials of mutated Flds with that of the WT indicated localized effects (*33*): either the appearance of small patches of positive electrostatic potential, Trp57Arg and Trp57Lys, or an even more negative surface in Trp57Glu (Figure 6A−D). The mutation of these residues also produced changes in the module and the orientation of the molecular dipole, which in *Anabaena* WT Fld is relatively strong and points its negative end toward the flavin ring (Figure 6G) (*18*). All these effects should contribute to the different binding and kinetic parameters when electrons are exchanged with FNR (Tables 1 and 2). Trp57Arg and Trp57Lys accepted electrons from FNR considerably faster than WT Fld (Tables 1 and 2) but noticeably hindered the reverse process (Table 2). This is consistent with their less negative $E_{ox/sq}$ and $E_{sq/hq}$ potentials (Figure 5) (*33*), which both facilitate the transfer of electrons from FNR and make FNR reduction by Fld more difficult. Trp57Glu produced much more moderated effects for both the forward and reverse processes (Tables 1 and 2), in agreement with the modest changes in its potentials (Figure 5). It is worth noting that previously reported data by replacement of Trp57 with other hydrophobic side chains produced much more moderate effects in both complex formation and ET processes (Tables 1 and 2) (*11*).

Replacement of the two hydrophobic Ile59 and Ile92 side chains, which are close to the FMN environment, spread to the solvent, and putatively located at the FNR:Fld interface (Figure 1A), with Ala or Glu produced slightly weaker interactions with FNR (Tables 1 and 2). Since these mutations are not expected to modify the FMN accessibility to the solvent (*33*), the changes in $\Delta\epsilon$ would probably be the result of different orientations between the redox centers in the mutated complexes. Introduction of Glu residues considerably increases the negative electrostatic potential around the isoalloxazine ring (Figure 6F) and modifies the Fld molecular dipole (Figure 6H). Moreover, replacement with Ala, and especially with Glu, also alters the shape of the protein surface (Figure 6E,F). Different shapes at the FNR interaction surface will be expected for these different Fld

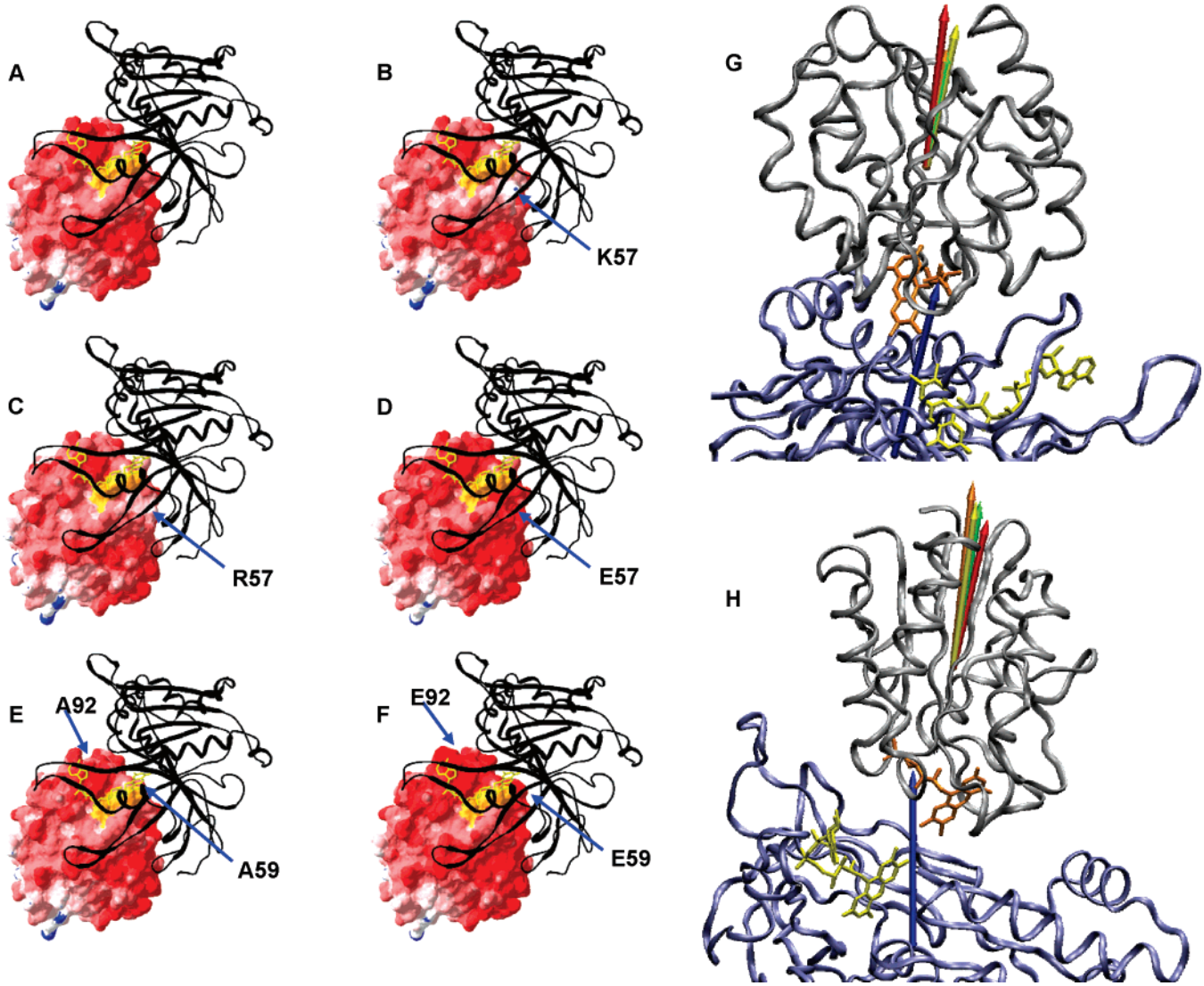

FIGURE 6: Influence of the mutations in the Fld electrostatic molecular surface and dipole moment. Electrostatic molecular surface representation of (A) WT, (B) Trp57Lys, (C) Trp57Arg, (D) Trp57Glu, (E) Ile59Ala/Ile92Ala, and (F) Ile59Glu/Ile92Glu Fld. An arrow shows localization of the introduced mutation on the protein surface. Negative potential is represented in red and positive potential in blue. The exposed surface of the FMN cofactor is drawn in orange. The position of FNR in the proposed model for the FNR−Fld interaction is shown by a black cartoon; its FAD group is represented in yellow sticks. The images were produced using SPDB-Viewer 3.7. Modification of the dipole moment magnitude and alignment for the Fld−FNR interaction for (G) WT (red), Trp57Glu (yellow), Trp57Lys (green), and Trp57Arg (orange) Flds and (H) WT (red), Ile59Glu (yellow), Ile92Glu (green), and Ile59Glu/Ile92Glu (orange) Flds. The ribbon models show the relative position of WT FNR (dark blue) and WT Fld (gray) in the reported model (*18*). The colored arrow indicates the position and magnitude of the dipole moment for each Fld form.

mutants, therefore promoting different orientations and distances between the Fld and FNR redox cofactors and contributing to different binding and ET properties. Subtle changes were also observed in the kinetic parameters. The single Fld mutants appeared slightly more efficient than WT Fld in accepting electrons from FNR_{hq}, and double mutants were less efficient (Tables 1 and 2). Although replacement of Ile59 and Ile92 by Ala or Glu makes $E_{ox/sq}$ considerably more negative than in WT Fld and $E_{sq/hq}$ slightly less negative (Figure 5) (*33*), it is expected that in all these Fld_{ox} mutants reduction to Fld_{sq} by FNR_{hq} or FNR_{sq} ($E_{ox/sq} = -385$ mV, $E_{sq/hq} = -371$ mV (*48*)), as well as reduction of both FNR_{ox} and FNR_{sq} by Fld_{hq}, will still be thermodynamically achieved.

Therefore, replacement of Trp57, Ile59, and Ile92 in Fld produces opposite effects depending on the introduced residue: some mutant Fld:FNR complexes can be weaker or less optimal for ET than those with WT Fld, but others can appear more optimized for a particular ET process (*3*). The Fld−FNR structural interaction model leads to a closest distance between the two flavin rings of ~4 Å (Figure 1) and suggests that Fld could adopt different orientations on the FNR surface without significantly altering the distance between the methyl groups of FAD and FMN (*4*, *18*). This might explain why subtle changes in the Fld surface, dipole moment, or midpoint reduction potentials still produce functional complexes with different binding and kinetic parameters. Moreover, the enhanced or hindered reactivity observed when some of the mutants are assayed can also be explained if there is a single orientation which is retained in any particular mutant that changes either the overall interaction or ET parameters. Therefore, this analysis indicates that in the *Anabaena* WT Fld−FNR ET interaction nonspecific transient collisions appear to play an important role in association, allowing multiple orientations and distances

between redox cofactors with efficient ET. Fld domains also play an important role in cellular metabolism in a large family of enzymes that also contain a C-terminal FNR domain and that probably arose due to an ancestral gene fusion event (*49*). These proteins, including NADPH-cytochrome P450 reductase, sulfite reductase, NADPH-dependent diflavin oxidoreductase 1, or methionine synthase reductase, are found in both prokaryotes and eukaryotes (including mammals), contain FAD and FMN, and shuttle electrons from NADPH to metal centers via their FNR and Fld domains (*49*−*53*). In these proteins flexibility of the Fld domain should be a requirement during ET, pivoting between the FNR domain and the metal domain (*49*). Despite the high structural homology between the Fld domains of these proteins and *Anabaena* Fld, residues Trp57, Ile59, and Ile92 do not show conservative replacements, usually being replaced with polar, and even charged, side chains. Additionally, the electronegative surface of these Fld domains is smaller with regard to Fld. Presumably, in dual-flavin reductases the fact of having covalently attached the different ET domains should eliminate the pressure to maintain strong electrostatic and hydrophobic contacts, allowing the required movement of the Fld domain to allow its action with both the FNR domain and the Fld domain electron acceptor (*49*). Thus, the more extensive electronegative surface at the interaction site and the hydrophobic patch around the FMN cofactor present in bacterial Flds appear to contribute to the selection of a bunch of encounter complexes with FNR able to evolve toward productive ET interactions.

A role of the FMN isoalloxazine ring in complex formation with FNR is also supported by our study, indicating that the closure of the flavin ring cavity by the hydrophobic Tyr94/Trp57 side chains (*34*) is not enough to produce a strong binding between ApoFld and FNR (Table 1, Figure 2). However, it remains to be proved whether this weaker affinity is the result of the removal of the interactions played by the benzene hydrophobic portion of FMN with FNR or whether it might be the result of the conformational changes observed in the FMN binding loops of Fld upon FMN removal (*34*).

As regards the interaction and ET between PSI_{rd} and Fld_{ox}, minor effects were observed upon replacement of Trp57 with Arg, but replacement with Glu considerably impaired the process. In its turn, Trp57Lys Fld presented a considerably enhanced ability to accept electrons from PSI at low $MgCl_2$ (Figure 4A,D). The increase in the ET rate of Trp57Lys Fld might relate to its less negative $E_{ox/sq}$ (Figure 5), but the behavior of Trp57Glu and Trp57Arg, as well as that of Trp57Lys at high $MgCl_2$, cannot be explained on such bases. The data for Trp57Lys Fld rather suggest a modified electrostatically driven interaction with PSI, in which complex rearrangement leading to an optimal orientation is attained at lower salt concentration. Such interaction does not appear to be achieved by the guanidinium group at the end of the long hydrophobic side chain of Arg in the Trp57Arg mutant, consistent with the different localization of both positive charges in the 3D models (Figure 6B,C) (*33*). Replacement of Trp57 with Phe, Ala, or Leu resulted in a behavior similar to the one described here for Trp57Lys, whereas introduction of a Tyr had a deleterious effect (Table 3) (*11*). A patch of hydrophobic residues has been proposed to be involved in Fd or Fld binding on the PSI PsaC subunit in the vicinity of F_B (*2*). Therefore, it could be hypothesized that the FMN exposed benzene ring portion and the Trp57 side chain would be located around this region in the PSI−Fld interaction. In such a case, changes in Trp57 in Fld would differently modify such an interaction, as it is actually observed (Figure 4A). The 3D models suggest an important increase in the negative electrostatic potential around FMN for Trp57Glu Fld, while it is considerably decreased in the Lys and Arg mutants, in which there are also changes in the magnitude and orientation of the molecular dipole relative to that of WT Fld (Figure 6G). However, replacement with residues of different nature still allows the formation of efficient ET complexes (Table 3) (*11*), indicating that Trp57 modulates the interaction but is not critically involved in the process. Thus, Trp57Lys, Trp57Phe, and Trp57Ala Flds produce complexes more optimized in accepting electrons from PSI_{rd} (Table 3) (*11*), whereas Trp57Arg only promotes slight effects at high salt concentration, suggesting changes in the hydrophobic forces involved in the interaction. The lack of reaction of Trp57Glu Fld with PSI_{rd} reflects the formation of a complex not compatible with ET, probably due to structural changes promoted by the less bulky negative group that enlarged the flavin area exposed to the solvent (*33*), in agreement with its also weaker interaction with FNR (Table 1).

Individual replacement of Ile92 with Ala or Glu results in the occurrence of a collisional-type mechanism with minor effects on the ET (as reported when replaced by Lys (*7*)). Ile59Ala/Ile92Ala and Ile59Ala Flds presented affinities for PSI_{rd} similar to that of WT Fld, but more efficient ET processes, especially the Ile59Ala mutant (Table 3). The introduction of a Glu at position 59 resulted in faster ET and in the occurrence of a collisional-type mechanism. Ile59Glu/Ile92Glu Fld binds tighter to PSI_{rd} than any other Fld variant, while also presenting a high k_{et} (Figure 4). These observations suggest that replacing Ile59 in WT Fld clearly contributes to improvement of ET from PSI_{rd}, whereas the residue at position 92 only modulates this behavior. The ionic strength dependence profiles of k_{obs} for Ile59Glu, Ile92Glu, and Ile59Glu/Ile92Glu (Figure 4D) suggest an additive effect of both mutations, less salt being required with the double mutant to allow the rearrangement to the optimal conformation for ET from PSI_{rd}. This is an unexpected result taking into account that Fld must interact with positive charges on PSI_{rd}. In addition, as a consequence of the double replacement of Ile59 and Ile92 with Glu, the net negative charge of the Fld surface increases and the molecular dipole suffers a change in orientation (Figure 6H). These are very likely additional factors in narrowing the ionic strength dependence curve for the double mutant. More generally, conformational changes in the PSI−Fld interactions due to the introduced modifications in the Fld surface leading to smaller or larger edge-to-edge distances between F_B and the FMN ring might also explain some of the observed effects. In this context we should also remember the ability of PSI to retain interaction specificity while demonstrating adaptability, allowing along its evolutionary process more than one protein to donate electrons at its reducing site (plastocyanin/cytochrome c_6) or to accept them at its oxidizing site (Fd/Fld) as well as evolving to more sophisticated kinetic mechanisms (*46*).

In conclusion, our data suggest that the side chains of Trp57, Ile59, and Ile92, as well as the conformational and hydrophobic properties conferred by FMN to its Fld environment, contribute to the productive orientation of the Fld complexes with FNR and PSI. However, the side chains of Trp57, Ile59, and Ile92 are not involved in crucial specific interactions. This supports the idea that the Fld interaction with its partners is less specific than that of Fd and that in the transient complexes more than one orientation can be efficient for ET (*3*, *4*, *7*). Such an idea is in agreement with recent experimental and theoretical studies that describe the dynamics of the assembly in macromolecular associations and the role played by transient collisions in ET protein−protein interactions producing populations of alternative encounter complexes (*47*, *54*). Additionally, the distance and mutual orientation between redox centers appear to be two of the principal factors governing ET in the Fld complexes. Therefore, for some of the analyzed reactions, WT Fld complexes with either FNR or PSI are not the most optimized ones for ET and some of the introduced particular mutations appear to favor single orientations which improve association and ET parameters with a particular partner. In addition to FNR and PSI, *Anabaena* Fld is involved in cyclic photosynthetic ET flow and interacts with a number of structurally different soluble proteins to introduce low redox potential electrons into cell metabolism for the assimilation of primordial bioelements. Additionally, the surfaces of Fld domains in dual-flavin reductases appear to have independently evolved from Fld for the function they have in each particular system. Therefore, it is feasible to think that the ancestral Fld adapted its surface to interact with different structural partners through nonspecific interactions, which in turn decreased the potential efficiency in ET that could be achieved if unique and more favorable orientations were produced with a reduced number of protein partners. This can be explained by assuming that the WT Fld complexes favor the interaction with very different redox partners rather than their kinetic efficiency.

ACKNOWLEDGMENT

We thank Jorge Estrada for his collaboration in the development of the program used in the calculation of the dipole moments.

REFERENCES

1. Rogers, L. J. (1987) Ferredoxins, flavodoxins and related proteins: structure, function and evolution, in *The Cyanobacteria* (Fay, P., and Van Baalen, C., Eds.) pp 35−67, Elsevier, Amsterdam.
2. Setif, P. (2006) Electron transfer from the bound iron-sulfur clusters to ferredoxin/flavodoxin: kinetic and structural properties of ferredoxin/flavodoxin reduction by photosystem I, in *Photosystem I. The Light-Driven Platocyanin:Ferredoxin Oxidoreductase* (Golbeck, J. H., Ed.) pp 439−454, Springer, Dordrecht, The Netherlands.
3. Nogues, I., Hervas, M., Peregrina, J. R., Navarro, J. A., de la Rosa, M. A., Gomez-Moreno, C., and Medina, M. (2005) *Anabaena* flavodoxin as an electron carrier from photosystem I to ferredoxin-$NADP^+$ reductase. Role of flavodoxin residues in protein-protein interaction and electron transfer, *Biochemistry 44*, 97−104.
4. Medina, M., and Gomez-Moreno, C. (2004) Interaction of ferredoxin-$NADP^+$ reductase with its substrates: Optimal interaction for efficient electron transfer, *Photosynth. Res. 79*, 113−131.
5. Hurley, J. K., Morales, R., Martinez-Julvez, M., Brodie, T. B., Medina, M., Gomez-Moreno, C., and Tollin, G. (2002) Structure-function relationships in *Anabaena* ferredoxin/ferredoxin-$NADP^+$ reductase electron transfer: insights from site-directed mutagenesis, transient absorption spectroscopy and X-ray crystallography, *Biochim. Biophys. Acta 1554*, 5−21.
6. Hurley, J. K., Tollin, G., Medina, M., and Gomez-Moreno, C. (2006) Electron transfer from ferredoxin and flavodoxin to ferredoxin-$NADP^+$ reductase, in *Photosystem I. The Light-Driven Platocyanin:Ferredoxin Oxidoreductase* (Golbeck, J. H., Ed.) pp 455−476, Springer, Dordrecht, The Netherlands.
7. Nogues, I., Martinez-Julvez, M., Navarro, J. A., Hervas, M., Armenteros, L., de la Rosa, M. A., Brodie, T. B., Hurley, J. K., Tollin, G., Gomez-Moreno, C., and Medina, M. (2003) Role of hydrophobic interactions in the flavodoxin mediated electron transfer from photosystem I to ferredoxin-$NADP^+$ reductase in *Anabaena* PCC 7119, *Biochemistry 42*, 2036−2045.
8. Martinez-Julvez, M., Medina, M., and Gomez-Moreno, C. (1999) Ferredoxin-$NADP^+$ reductase uses the same site for the interaction with ferredoxin and flavodoxin, *J. Biol. Inorg. Chem. 4*, 568−578.
9. Martinez-Julvez, M., Medina, M., Hurley, J. K., Hafezi, R., Brodie, T. B., Tollin, G., and Gomez-Moreno, C. (1998) Lys75 of *Anabaena* ferredoxin-$NADP^+$ reductase is a critical residue for binding ferredoxin and flavodoxin during electron transfer, *Biochemistry 37*, 13604−13613.
10. Martinez-Julvez, M., Nogues, I., Faro, M., Hurley, J. K., Brodie, T. B., Mayoral, T., Sanz-Aparicio, J., Hermoso, J. A., Stankovich, M. T., Medina, M., Tollin, G., and Gomez-Moreno, C. (2001) Role of a cluster of hydrophobic residues near the FAD cofactor in *Anabaena* PCC 7119 ferredoxin-$NADP^+$ reductase for optimal complex formation and electron transfer to ferredoxin, *J. Biol. Chem. 276*, 27498−27510.
11. Casaus, J. L., Navarro, J. A., Hervas, M., Lostao, A., De la Rosa, M. A., Gomez-Moreno, C., Sancho, J., and Medina, M. (2002) *Anabaena* sp. PCC 7119 flavodoxin as electron carrier from photosystem I to ferredoxin-$NADP^+$ reductase. Role of Trp(57) and Tyr(94), *J. Biol. Chem. 277*, 22338−22344.
12. De Pascalis, A. R., Jelesarov, I., Ackermann, F., Koppenol, W. H., Hirasawa, M., Knaff, D. B., and Bosshard, H. R. (1993) Binding of ferredoxin to ferredoxin:$NADP^+$ oxidoreductase: the role of carboxyl groups, electrostatic surface potential, and molecular dipole moment, *Protein Sci. 2*, 1126−1135.
13. Meimberg, K., Fischer, N., Rochaix, J. D., and Muhlenhoff, U. (1999) Lys35 of PsaC is required for the efficient photoreduction of flavodoxin by photosystem I from *Chlamydomonas reinhardtii*, *Eur. J. Biochem. 263*, 137−144.
14. Setif, P., Fischer, N., Lagoutte, B., Bottin, H., and Rochaix, J. D. (2002) The ferredoxin docking site of photosystem I, *Biochim. Biophys. Acta 1555*, 204−209.
15. Setif, P. (2001) Ferredoxin and flavodoxin reduction by photosystem I, *Biochim. Biophys. Acta 1507*, 161−179.
16. Morales, R., Charon, M. H., Kachalova, G., Serre, L., Medina, M., Gomez-Moreno, C., and Frey, M. (2000) A redox-dependent interaction between two electron-transfer partners involved in photosynthesis, *EMBO Rep. 1*, 271−276.
17. Kurisu, G., Kusunoki, M., Katoh, E., Yamazaki, T., Teshima, K., Onda, Y., Kimata-Ariga, Y., and Hase, T. (2001) Structure of the electron transfer complex between ferredoxin and ferredoxin-$NADP^+$ reductase, *Nat. Struct. Biol. 8*, 117−121.
18. Mayoral, T., Martinez-Julvez, M., Perez-Dorado, I., Sanz-Aparicio, J., Gomez-Moreno, C., Medina, M., and Hermoso, J. A. (2005) Structural analysis of interactions for complex formation between ferredoxin-$NADP^+$ reductase and its protein partners, *Proteins 59*, 592−602.
19. Lostao, A., Gomez-Moreno, C., Mayhew, S. G., and Sancho, J. (1997) Differential stabilization of the three FMN redox forms by tyrosine 94 and tryptophan 57 in flavodoxin from *Anabaena* and its influence on the redox potentials, *Biochemistry 36*, 14334−14344.
20. Hoover, D. M., and Ludwig, M. L. (1997) A flavodoxin that is required for enzyme activation: the structure of oxidized flavodoxin from *Escherichia coli* at 1.8 Å resolution, *Protein Sci. 6*, 2525−2537.
21. Rao, S. T., Shaffie, F., Yu, C., Satyshur, K. A., Stockman, B. J., Markley, J. L., and Sundarlingam, M. (1992) Structure of the oxidized long-chain flavodoxin from *Anabaena* 7120 at 2 Å resolution, *Protein Sci. 1*, 1413−1427.
22. Drennan, C. L., Pattridge, K. A., Weber, C. H., Metzger, A. L., Hoover, D. M., and Ludwig, M. L. (1999) Refined structures of oxidized flavodoxin from *Anacystis nidulans*, *J. Mol. Biol. 294*, 711−724.

23. Fukuyama, K., Wakabayashi, S., Matsubara, H., and Rogers, L. J. (1990) Tertiary structure of oxidized flavodoxin from an eukaryotic red alga *Chondrus crispus* at 2.35-Å resolution. Localization of charged residues and implication for interaction with electron transfer partners, *J. Biol. Chem. 265*, 15804−15812.
24. Watt, W., Tulinsky, A., Swenson, R. P., and Watenpaugh, K. D. (1991) Comparison of the crystal structures of a flavodoxin in its three oxidation states at cryogenic temperatures, *J. Mol. Biol. 218*, 195−208.
25. Alagaratnam, S., van Pouderoyen, G., Pijning, T., Dijkstra, B. W., Cavazzini, D., Rossi, G. L., Van Dongen, W. M., van Mierlo, C. P., van Berkel, W. J., and Canters, G. W. (2005) A crystallographic study of Cys69Ala flavodoxin II from *Azotobacter vinelandii*: structural determinants of redox potential, *Protein Sci. 14*, 2284−2295.
26. Drummond, M. H. (1985) The base sequence of the nifF gene of *Klebsiella pneumoniae* and homology of the predicted amino acid sequence of its protein product to other flavodoxins, *Biochem. J. 232*, 891−896.
27. Ludwig, M. L., Pattridge, K. A., Metzger, A. L., Dixon, M. M., Eren, M., Feng, Y., and Swenson, R. P. (1997) Control of oxidation-reduction potentials in flavodoxin from *Clostridium beijerinckii*: the role of conformation changes, *Biochemistry 36*, 1259−1280.
28. Freigang, J., Diederichs, K., Schafer, K. P., Welte, W., and Paul, R. (2002) Crystal structure of oxidized flavodoxin, an essential protein in *Helicobacter pylori*, *Protein Sci. 11*, 253−261.
29. Hu, Y., Li, Y., Zhang, X., Guo, X., Xia, B., and Jin, C. (2006) Solution structures and backbone dynamics of a flavodoxin mioC from *Escherichia coli* in both apo- and holo- forms: Implications for cofactor binding and electron transfer, *J. Biol. Chem. 281*, 35454−35466.
30. Muhlenhoff, U., Kruip, J., Bryant, D. A., Rogner, M., Setif, P., and Boekema, E. (1996) Characterization of a redox-active cross-linked complex between cyanobacterial photosystem I and its physiological acceptor flavodoxin, *EMBO J. 15*, 488−497.
31. Chitnis, V. P., Jungs, Y. S., Albee, L., Golbeck, J. H., and Chitnis, P. R. (1996) Mutational analysis of photosystem I polypeptides. Role of PsaD and the lysyl 106 residue in the reductase activity of the photosystem I, *J. Biol. Chem. 271*, 11772−11780.
32. Navarro, J. A., Hervas, M., Genzor, C. G., Cheddar, G., Fillat, M. F., de la Rosa, M. A., Gomez-Moreno, C., Cheng, H., Xia, B., Chae, Y. K., and et al. (1995) Site-specific mutagenesis demonstrates that the structural requirements for efficient electron transfer in *Anabaena* ferredoxin and flavodoxin are highly dependent on the reaction partner: kinetic studies with photosystem I, ferredoxin-$NADP^+$ reductase, and cytochrome *c*, *Arch. Biochem. Biophys. 321*, 229−238.
33. Frago, S., Goñi, G., Herguedas, B., Peregrina, J. R., Serrano, A., Perez-Dorado, I., Molina, R., Gómez-Moreno, C., Hermoso, J. A., Martínez-Júlvez, M., Mayhew, S. G., and Medina, M. (2007) Tuning of the FMN binding and oxido-reduction properties by neighboring side-chains in *Anabaena* Flavodoxin, *Arch. Biochem. Biophys. 467*, 206−217.
34. Genzor, C. G., Perales-Alcon, A., Sancho, J., and Romero, A. (1996) Closure of a tyrosine/tryptophan aromatic gate leads to a compact fold in apoflavodoxin, *Nat. Struct. Biol. 3*, 329−332.
35. Edmondson, D. E., and Tollin, G. (1971) Chemical and physical characterization of the Shethna flavoprotein and apoprotein and kinetics and thermodynamics of flavin analog binding to the apoprotein, *Biochemistry 10*, 124−132.
36. Medina, M., Martinez-Julvez, M., Hurley, J. K., Tollin, G., and Gomez-Moreno, C. (1998) Involvement of glutamic acid 301 in the catalytic mechanism of ferredoxin-$NADP^+$ reductase from *Anabaena* PCC 7119, *Biochemistry 37*, 2715−2728.
37. Pueyo, J. J., and Gomez-Moreno, C. (1991) Purification of ferredoxin-$NADP^+$ reductase, flavodoxin and ferredoxin from a single batch of the cyanobacterium *Anabaena* PCC 7119, *Prep. Biochem. 21*, 191−204.
38. Medina, M., Hervas, M., Navarro, J. A., De la Rosa, M. A., Gomez-Moreno, C., and Tollin, G. (1992) A laser flash absorption spectroscopy study of *Anabaena* sp. PCC 7119 flavodoxin photoreduction by photosystem I particles from spinach, *FEBS Lett. 313*, 239−242.
39. Hervas, M., Navarro, J. A., Diaz, A., Bottin, H., and De la Rosa, M. A. (1995) Laser-flash kinetic analysis of the fast electron transfer from plastocyanin and cytochrome c_6 to photosystem I. Experimental evidence on the evolution of the reaction mechanism, *Biochemistry 34*, 11321−11326.
40. Meyer, T. E., Zhao, Z. G., Cusanovich, M. A., and Tollin, G. (1993) Transient kinetics of electron transfer from a variety of c-type cytochromes to plastocyanin, *Biochemistry 32*, 4552−4559.
41. Guex, N., and Peitsch, M. C. (1997) SWISS-MODEL and the Swiss-PdbViewer: an environment for comparative protein modeling, *Electrophoresis 18*, 2714−2723.
42. Case, D. A., Cheatham, T. E., III, Darden, T., Gohlke, H., Luo, R., Merz, K. M., Jr., Onufriev, A., Simmerling, C., Wang, B., and Woods, R. J. (2005) The Amber biomolecular simulation programs, *J. Comput. Chem. 26*, 1668−1688.
43. Schneider, C., and Suhnel, J. (1999) A molecular dynamics simulation of the flavin mononucleotide-RNA aptamer complex, *Biopolymers 50*, 287−302.
44. Myers, J., Grothaus, G., Narayanan, S., and Onufriev, A. (2006) A simple clustering algorithm can be accurate enough for use in calculations of pKs in macromolecules, *Proteins 63*, 928−938.
45. Gordon, J. C., Myers, J. B., Folta, T., Shoja, V., Heath, L. S., and Onufriev, A. (2005) H++: a server for estimating pK_{as} and adding missing hydrogens to macromolecules, *Nucleic Acids Res. 33*, W368−371.
46. Hervas, M., Navarro, J. A., and De La Rosa, M. A. (2003) Electron transfer between membrane complexes and soluble proteins in photosynthesis, *Acc. Chem. Res. 36*, 798−805.
47. Blundell, T. L., and Fernandez-Recio, J. (2006) Cell biology—Brief encounters bolster contacts, *Nature 444*, 279−280.
48. Nogues, I., Tejero, J., Hurley, J. K., Paladini, D., Frago, S., Tollin, G., Mayhew, S. G., Gomez-Moreno, C., Ceccarelli, E. A., Carrillo, N., and Medina, M. (2004) Role of the C-terminal tyrosine of ferredoxin-nicotinamide adenine dinucleotide phosphate reductase in the electron transfer processes with its protein partners ferredoxin and flavodoxin, *Biochemistry 43*, 6127−6137.
49. Gruez, A., Pignol, D., Zeghouf, M., Coves, J., Fontecave, M., Ferrer, J. L., and Fontecilla-Camps, J. C. (2000) Four crystal structures of the 60 kDa flavoprotein monomer of the sulfite reductase indicate a disordered flavodoxin-like module, *J. Mol. Biol. 299*, 199−212.
50. Wang, M., Roberts, D. L., Paschke, R., Shea, T. M., Masters, B. S., and Kim, J. J. (1997) Three-dimensional structure of NADPH-cytochrome P450 reductase: prototype for FMN- and FAD-containing enzymes, *Proc. Natl. Acad. Sci. U.S.A. 94*, 8411−8416.
51. Panda, K., Haque, M. M., Garcin-Hosfield, E. D., Durra, D., Getzoff, E. D., and Stuehr, D. J. (2006) Surface charge interactions of the FMN module govern catalysis by nitric-oxide synthase, *J. Biol. Chem. 281*, 36819−36827.
52. Wolthers, K. R., and Scrutton, N. S. (2007) Protein interactions in the human methionine synthase-methionine synthase reductase complex and implications for the mechanism of enzyme reactivation, *Biochemistry 46*, 6696−6709.
53. Sibille, N., Blackledge, M., Brutscher, B., Coves, J., and Bersch, B. (2005) Solution structure of the sulfite reductase flavodoxin-like domain from, *Escherichia coli*, *Biochemistry 44*, 9086−9095.
54. Muresanu, L., Pristovsek, P., Lohr, F., Maneg, O., Mukrasch, M. D., Ruterjans, H., Ludwig, B., and Lucke, C. (2006) The electron transfer complex between cytochrome c_{552} and the CuA domain of the *Thermus thermophilus* ba_3 oxidase. A combined NMR and computational approach, *J. Biol. Chem. 281*, 14503−14513.

BI7017392